Available online at www.sciencedirect.com
ScienceDirect
Scripta Materialia 56 (2007) 1047–1050
Scripta MATERIALIA
www.elsevier.com/locate/scriptamat

Severe plastic deformation of copper by machining: Microstructure refinement and nanostructure evolution with strain

S. Swaminathan,[a] T.L. Brown,[b] S. Chandrasekar,[b] T.R. McNelley[a,*] and W.D. Compton[b]

[a] *Department of Mechanical and Astronautical Engineering, Naval Postgraduate School, Monterey, CA 93943-5146, USA*
[b] *School of Industrial Engineering, Purdue University, West Lafayette, IN 47907-2023, USA*

Received 30 December 2006; revised 20 February 2007; accepted 24 February 2007
Available online 6 April 2007

The microstructures of copper chips created by plane strain machining at ambient temperature have been analyzed using transmission electron microscopy (TEM) and orientation imaging microscopy (OIM). The strain imposed in the chips was varied by changing the tool rake angle. Characterization of orthogonal faces of the chips showed the microstructure to be essentially uniform through the chip volume, indicative also of uniform deformation.
Published by Elsevier Ltd. on behalf of Acta Materialia Inc.

Keywords: Machining; Copper; Severe plastic deformation; Microstructure; Microtexture

Imposition of large plastic strains in bulk materials is a well-known method for promoting formation of ultra-fine grained (UFG) and nanocrystalline microstructures [1–8]. Equal channel angular pressing [1,2], high-pressure torsion [3], rolling [4] and wire drawing [5,6] have been routinely employed as severe plastic deformation (SPD) processes for introducing large strains. Typically, these processes involve multiple passes of deformation with changes in orientation of deformation between passes. Microstructure refinement in bulk materials can also be realized by the process of chip formation as in plane strain machining [7,8]. In machining, large plastic strains of 1–15 are introduced into the chip in a single pass of deformation. While SPD and microstructure refinement by machining have been demonstrated in a variety of material systems ranging from low to high initial strength, the uniformity of microstructure through the volume of a chip has not been assessed to date. This aspect, which is essential for establishing scalability of machining as a class of processes for making bulk nanostructured materials, is addressed in the present study using copper as a model material system.

Figure 1 is a schematic of chip formation in plane strain machining, wherein the chip material being removed by large strain deformation slides over the rake face of the tool. The principal machining parameters are the tool rake angle, α, the undeformed chip thickness, a_0, the deformed chip thickness, a_c, and the cutting velocity, V_0 (Fig. 1). The shear strain, γ, imposed in the chip depends on α and the shear plane angle, φ, and can be estimated as [9]

$$\gamma = \frac{\cos(\alpha)}{\sin(\varphi)\cos(\varphi - \alpha)} \tag{1}$$

where φ depends on α and cutting ratio r ($=a_0/a_c$) as

$$\tan(\varphi) = \frac{r\cos(\alpha)}{1 - r\sin(\alpha)} \tag{2}$$

Plastic shear strain values in the chip typically range from 1 to 15 and can be varied by changing the tool rake angle. The cutting velocity, V_0, controls the strain rate and temperature of the process. At low values of V_0, chip formation occurs at near-ambient temperature. However, at very high values of V_0, temperatures of the order of the melting point of the material and strain rates as high as $1 \times 10^5\ s^{-1}$ are known to prevail in the deformation zone [10]. Conditions of plane strain deformation exist when the tool cutting edge is perpendicular to V_0, and a_0 is small compared to the chip width, a_w.

Chips were produced by plane strain machining of commercial oxygen-free high-conductivity (OFHC) copper. For this purpose, an OFHC copper rod 150 mm long and 25.4 mm in diameter was annealed at 400 °C for 4 h in a controlled argon atmosphere (95 vol.% Ar + 5 vol.% H_2). The annealed copper's (bulk) microstructure consisted of ~100 μm grains with

* Corresponding author. E-mail: TMcNelley@nps.edu

1359-6462/$ - see front matter Published by Elsevier Ltd. on behalf of Acta Materialia Inc.
doi:10.1016/j.scriptamat.2007.02.034

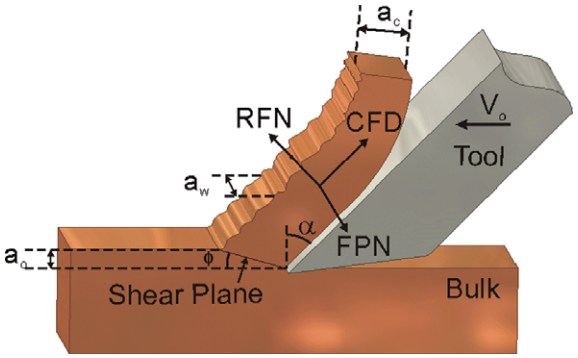

Figure 1. Schematic of chip formation in plane strain machining and directions used in OIM analysis. RFN is normal to the tool rake face, CFD is along the direction of chip flow and FPN is the direction transverse to the chip flow direction (principal strain = 0 parallel to FPN).

annealing twins, and microtexture data revealed a weak cube component in the texture. Chips were produced with different levels of strain using high-speed steel tools of different rake angles (+40°, +20° or 0°). The machining parameters used were $a_0 = 0.1$ mm, $a_w = 3.8$ mm and $V_0 = 18.3$ mm s^{-1} (see Table 1). For these parameters, the strain rate in the chip was in the range of 10–100 s^{-1} [10] and deformation occurred under near-ambient temperature conditions. The deformed chip thickness, a_c, was measured, from which r, φ, and γ were estimated using Eqs. (1) and (2); these parameter values are summarized in Table 1. Typical chip samples were 4 mm in width, 0.3–1.0 mm in thickness and at least 50 mm in length. For transmission electron microscopy (TEM) observations, samples were prepared using a twin-jet Struers Tenupol 5 with a solution of 46 vol.% H_3PO_4 in water at 20 °C and an operating voltage of 5.5 V. Bright-field images and corresponding selected area diffraction (SAD) patterns were taken (with aperture size of 6.7 μm) using a JEOL-2000FX microscope operating at 200 kV with a LaB_6 filament. If the aspect ratio was greater than 2, the structures were considered elongated; otherwise they were considered equiaxed. For orientation imaging microscopy (OIM) analysis, three mutually orthogonal faces of the chips (the directions normal to these faces are designated as chip flow direction (CFD), rake face normal (RFN) and flow plane normal (FPN), as shown in Fig. 1) were metallographically prepared and then electropolished using 85 vol.% H_3PO_4 in water at 12 V. These faces were then observed and analyzed by SEM using OIM. An idealized model of plane strain machining involves simple shear distortion in the flow plane, which is defined by the RFN and the CFD. Thus, the symmetry of the process is monoclinic with the 2-fold rotation axis aligned with the FPN, and care was therefore taken to identify the different planes and their orientations during the mounting of samples in the scanning electron microscope. The OIM was conducted in a TOPCON S-510 scanning electron microscope operating at 20 kV with a tungsten filament with a step-size of 0.3 μm. The OIM study involved standard clean-up procedures [11]: (i) grain dilatation with a grain tolerance angle (GTA) of 5°; a minimum grain size (MGS) of two pixels; (ii) grain confidence index (CI) standardization with GTA = 5° and MGS = 2; and (iii) neighbor CI correlation with minimum CI of 0.1.

TEM observations taken in the rake face plane are provided in Figures 2 and 3 to illustrate the effect of strain. In a chip deformed to a low shear strain ($\gamma \sim 3$) prior grain boundaries and dislocations are apparent in Figure 2a while elongated, ultra-fine dislocation structures are evident elsewhere in the foil, as shown in Figure 2b. Upon deformation to a strain of ~7 the original grain boundaries are no longer discernible and the microstructure consists of elongated, nanostructures that also contain dislocation tangles, as may be seen in Figure 3a. When the strain is increased to ~11 the microstructure consists predominantly of equiaxed nanoscale structures; the interiors of these features are largely free of dislocations, as seen in Figure 3b. The spreading of spots in the inset SAD patterns in Figures 2 and 3 suggest that the misorientations of the structure boundaries increase with strain.

Table 1. Machining and deformation parameters

V_0 (mm s^{-1})	a_0 (mm)	a_w (mm)	α	r	φ	γ
18.3	0.11	3.81	+40°	0.31	16.4°	3
			+20°	0.14	8.0°	7
			0°	0.09	5.2°	11

The cutting ratio, r, is measured experimentally; the values of shear plane angle, φ, and shear strain, γ, are estimated using Eqs. (1) and (2).

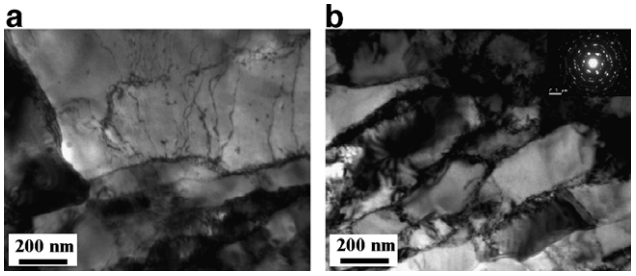

Figure 2. TEM images of copper chips subjected to a strain of $\gamma \sim 3$ showing the presence of (a) original grain boundaries with dislocation structures developing within grains and (b) elongated, ultra-fine structures. The TEM sample faces are parallel to the rake face plane.

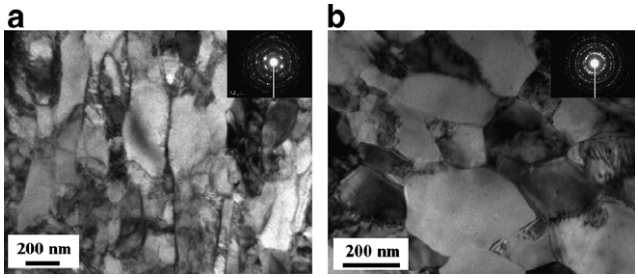

Figure 3. TEM images of copper chips subjected to strains of (a) $\gamma \sim 7$, showing elongated nanostructures; and (b) $\gamma \sim 11$, showing equiaxed nanostructures. The TEM sample faces are parallel to the rake face plane.

The OIM data for each of these three shear strains are shown in Figure 4. In each case, inverse pole figure maps were determined for data from each of the three orthogonal chip faces and triplanar montages were then prepared to illustrate the evolution of microstructure in the volume of each of these chips. For each strain the results from the rake face plane (i.e. the CFD–FPN plane) are in consonance with the TEM data. Large, internally subdivided grains transform to elongated structures and, finally, to equiaxed structures as the strain levels increase (Fig. 4a–c). It is noteworthy that, at each strain level, the microstructure data from each of the three

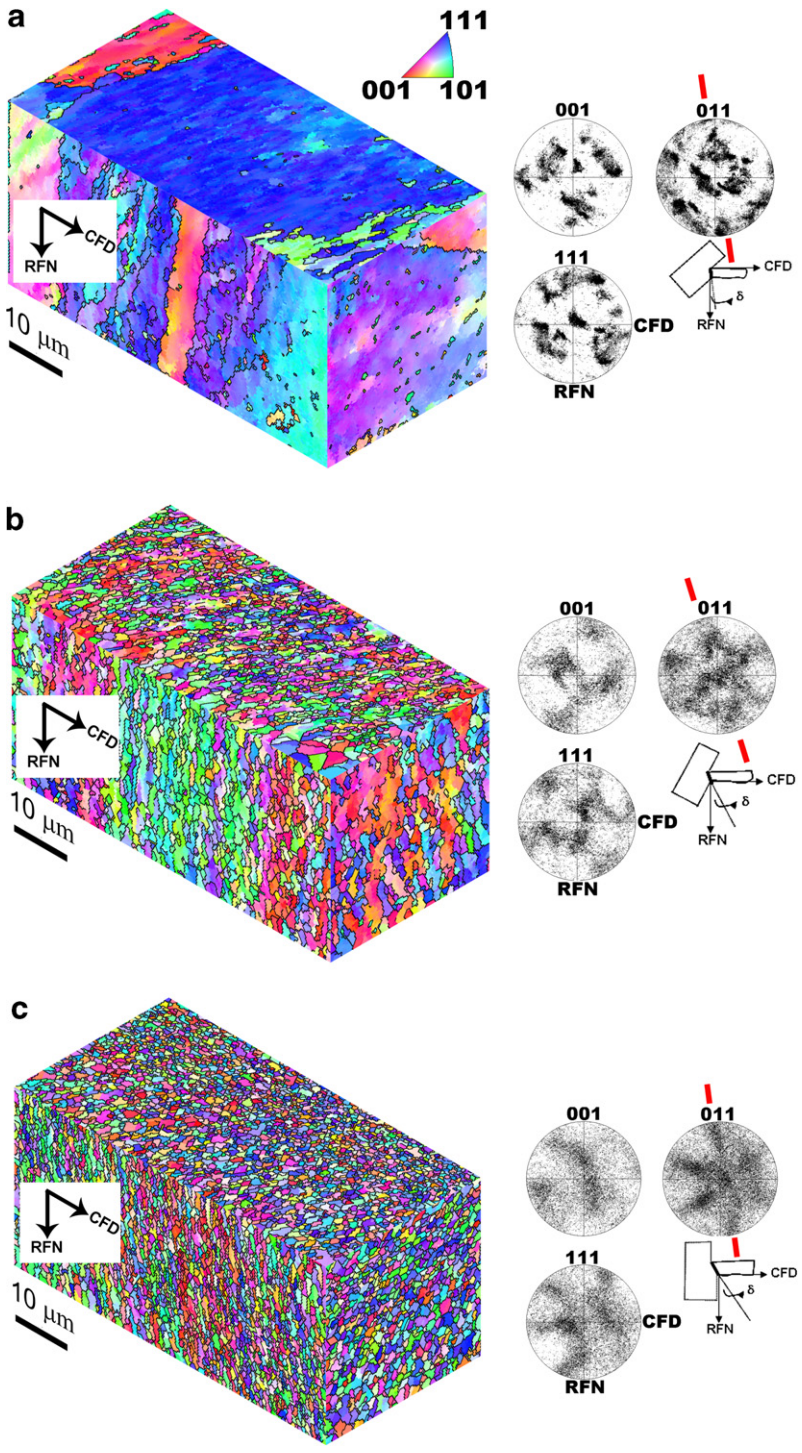

Figure 4. Triplanar OIM images of copper chips subjected to strains of (a) $\gamma \sim 3$, showing the presence of original grain boundaries with structures within grains as delineated by color variation (pole figure data showing predominantly B-fiber shear textures); (b) $\gamma \sim 7$, showing presence of elongated, ultra-fine structures and absence of original grain boundaries (the pole figures display A and B-fiber shear textures); and (c) $\gamma \sim 11$, showing equiaxed ultra-fine structures with B-fibers and distinct C-components in the shear texture. The dotted line on the (0 1 1) pole figure gives the observed shear direction; δ is the angle made by the shear plane with RFN, and increases with decreasing rake angle, α.

orthogonal faces of each sample are very similar, indicating uniformity of microstructure throughout the chip volume. Such a uniform microstructure would imply that the deformation is also uniform throughout the chip, consistent with strain measurements carried out in chips using a particle image velocimetry technique [10]. Altogether, these data show that the population of high-angle boundaries ($\geqslant 15°$ misorientation and indicated by the dark lines in Fig. 4) increases as the imposed strain level increases. For example, the fraction of high-angle boundaries in the RFN–CFD plane increases from 22.7% to 53.4% to 72% as the strain level increases from 3 to 7 to 11, respectively, in Figure 4. The discrete pole figures that are also shown in Figure 4 were calculated in each case from the data acquired on the RFN–CFD plane (this is the flow plane for simple shear); the orientation and senses of these axes as well as the approximate shear plane orientation are indicated in the insets with the pole figures. The pole figure data all include characteristic shear deformation components. At the location of the data of Figure 4a, which corresponds to a strain of ~3, the texture comprises two distinct variants of B-fiber component, i.e. $(1\,1\,2)[1\,-1\,0]$ and $(2\,1\,1)[0\,-1\,1]$, where the notation refers to (plane parallel to the shear plane of the machining)[direction parallel to the shear direction of machining] [12]. A rotated cube component reflecting the texture of the bulk material may also be discerned. The texture is inhomogeneous at the scale of the data in Figure 4a and other B-fiber orientations as well as the C component are observed elsewhere in this sample, probably a reflection of the coarse initial grain size of the material. For the sample that had experienced a strain of ~7 the pole figures shown in Figure 4b indicate more nearly continuous distributions of orientations along the A and B shear texture fibers when compared to results for a strain of ~3. In particular, prominent orientations include an A fiber orientation near $(1\,1\,1)[-1\,-1\,2]$ as well as an orientation near the intersection of the A and B fiber, i.e. $(1\,1\,1)[0\,-1\,1]$. Furthermore the textures are more nearly homogeneous in the volume of the chip and the cube component is not discernible. A shear texture is still evident upon increasing the strain to ~11; at this strain, the microstructure comprises of equiaxed structures. The pole figure in Figure 4c includes B-fiber orientations and a distinct C-type shear texture component, i.e. $\{1\,0\,0\}\langle 1\,1\,0\rangle$, as well as random orientations. These latter orientations like arise from lattice rotation within equiaxed structures that evolve at large deformation strains. Pole figures acquired from other orthogonal planes give results consistent with those of Figure 4.

In summary, TEM analysis shows that increasing the strain imposed during chip formation causes grain refinement leading to nanocrystalline materials. OIM observations on mutually orthogonal chip faces indicate that the microstructure and, hence, the deformation are essentially uniform throughout the volume of the chips. Corresponding pole figures reveal the presence of shear textures and the persistence of these deformation-induced textures even up to shear strains of ~11. The OIM data are also consistent with the TEM observations for the specific orientation in which the samples were examined under the transmission electron microscope.

These preliminary observations pertaining to uniformity of microstructure in the chip are particularly encouraging for the development of various geometrically constrained machining processes (e.g. large strain extrusion machining (LSEM)) as a means for producing bulk nanostructured materials [13]. In LSEM, the geometry and dimension of the chip are directly controlled at the point of its formation while large plastic strains are simultaneously imposed effecting microstructure refinement. Consequently, bulk nanostructured materials in the form of sheet, bar and foil can be produced by this controlled chip formation process in a variety of material systems [13]. The observed uniformity of the microstructure (and deformation) over the sample volume suggests that these machining processes are very likely scalable for making bulk forms with UFG and nanocrystalline microstructures.

The work at Purdue was supported by the US Department of Energy (grant 4000031768 via University of Tennessee – Batelle), Oak Ridge National Laboratory (ORNL), the State of Indiana's 21st Century Research and Technology Fund, and the NSF (grant CMMI-0626047). The work at NPS was partially supported by the US Air Force Office of Scientific Research under funding document no. F1ATA06058G001. S.S. would like to acknowledge a National Research Council Fellowship. The authors would like to thank Mr. Juan María García de la Infanta from Centro Nacional de Investigaciones Metalurgicas (CENIM), Spain for help with preparation of Figures 1 and 4.

[1] V.M. Segal, V.I. Reznikov, A.E. Drobyshevskiy, V.I. Kopylov, Russ. Metall. 1 (1981) 99.
[2] O.V. Mishin, D. Juul Jensen, N. Hansen, Mater. Sci. Eng. A 342 (2003) 320.
[3] A.P. Zhilyaev, S. Lee, G.V. Nurislamova, R.Z. Valiev, T.G. Langdon, Scripta Mater. 44 (2001) 2753.
[4] D.A. Hughes, N. Hansen, Acta Mater. 48 (11) (2000) 2985.
[5] J.D. Embury, R.M. Fisher, Acta Metall. 14 (1966) 147.
[6] G. Langford, M. Cohen, Trans. ASM 62 (1969) 623.
[7] T.L. Brown, S. Swaminathan, S. Chandrasekar, W.D. Compton, A.H. King, K.P. Trumble, J. Mater. Res. 17 (10) (2002) 2484.
[8] S. Swaminathan, M. Ravi Shankar, S. Lee, J. Hwang, A.H. King, R.F. Kezar, B.C. Rao, T.L. Brown, S. Chandrasekar, W.D. Compton, K.P. Trumble, Mater. Sci. Eng. A 410–411 (2005) 358.
[9] M.C. Shaw, Metal Cutting Principles, Oxford University Press, Oxford, 1984.
[10] S. Lee, J. Hwang, M. Ravi Shankar, S. Chandrasekar, W.D. Compton, Metall. Mater. Trans. A 37 (2006) 1633.
[11] A.P. Zhilyaev, K. Oh-ishi, G.I. Raab, T.R. McNelley, in: Y.T. Zhu et al. (Eds.), Ultrafine Grained Materials IV, TMS, Warrendale, PA, 2006, p. 113.
[12] G.R. Canova, U.F. Kocks, J.J. Jonas, Acta Metall. 32 (1984) 211.
[13] W. Moscoso, M. Ravi Shankar, J.B. Mann, W.D. Compton, S. Chandrasekar, J. Mater. Res. 22 (2007) 201.